Variability in infragravity wave processes during estuary artificial entrance openings

Article *in* Earth Surface Processes and Landforms · August 2020

DOI: 10.1002/esp.4974

3 authors, including:

Sarah Mcsweeney
University of Canterbury
24 PUBLICATIONS **211** CITATIONS
SEE PROFILE

Justin C Stout
University of Canterbury
27 PUBLICATIONS **303** CITATIONS
SEE PROFILE

McSweeney Sarah (Orcid ID: 0000-0003-0442-7426)

KENNEDY DAVID (Orcid ID: 0000-0002-4878-7717)

Variability in infragravity wave processes during estuary artificial entrance openings.

Sarah L. McSweeney[1], Justin C. Stout[1,2], and David M. Kennedy[1]

[1]School of Geography, The University of Melbourne, 221 Bouverie Street, Carlton, 3010, Victoria, Australia

[2]PrESM Research Group, Griffith Centre for Coastal Management, Griffith University, Gold Coast, 4215, Queensland, Australia

Corresponding author:

Sarah L. McSweeney

Address: School of Geography, The University of Melbourne, 221 Bouverie Street, Carlton, 3010, Victoria, Australia

Email: sarah.mcsweeney@unimelb.edu.au

Phone: +61 3 9035 9781

Running head: Infragravity wave processes during an estuary opening.

This article has been accepted for publication and undergone full peer review but has not been through the copyediting, typesetting, pagination and proofreading process which may lead to differences between this version and the Version of Record. Please cite this article as doi: 10.1002/esp.4974

Abstract: Intermittently Open/Closed Estuaries (IOCE) are wave-dominated estuaries with entrances which temporarily close to the ocean. Wave-current interactions play a major role in estuary entrance morphodynamics and influence the degree of energy transfer from the ocean into the lagoon. This study utilises artificial entrance openings of multiple ICOE in Victoria, Australia, to capture continuous hydrodynamic and geomorphic data throughout the opening cycle. We illustrate that water level oscillations in the infragravity (IG) band) are present in the basin during open entrance conditions. IG waves were observed to propagate up to 1.8 km upstream of the mouth while the entrance was open. Our work identifies that changes in cross-sectional area, bed depth at the berm position, and offshore wave height control the magnitude of IG waves within the estuary basin. IG wave magnitude is also tidally modulated and increases with high tides when the nearshore water level is higher. Late during the drainage phase, waves were observed to track the margins of the channel, away from the thalweg, and reach the basin. IG wave energy was highest immediately after the basin had ceased draining and while channel dimensions at the mouth were within 10% of their maximum value. As the entrance aggrades, IG wave magnitude decreases in the absence of energetic offshore wave conditions. We relate the changes in IG wave magnitude and frequency to a six-stage conceptual model of the opening-closure sequence. Within the basin, IG wave energy, height, and frequency were also consistently highest closer to the mouth and decreased with distance upstream. Our findings indicate that water level oscillations in the IG band are a persistent feature in IOCE and may be the norm rather than the exception in these systems. As IG waves were captured serendipitously as part of a larger field campaign, future work will focus on instrumenting IOCE to gain high resolution data to quantify IG wave processes during entrance openings.

Keywords: estuary, infragravity waves, waves, coastal lagoon, estuary morphodynamics

1.0 Introduction

Intermittently Open/Closed Estuaries (IOCE) are wave-dominated estuaries characterised by periodic entrance closure. IOCE comprise approximately 15% of all estuaries globally on microtidal to low-mesotidal coasts, often fronting rivers with low or variable flow regimes (McSweeney et al., 2017). IOCE entrance condition is controlled by the relative balance between on and offshore sediment transport at the mouth (Hanes et al., 2011; Behrens et al., 2013). Closure occurs when onshore sediment delivery from wave processes exceeds the seaward transport capacity of the ebb-tidal prism (Ranasinghe and Pattiaratchi, 1999; 2003). Entrance opening occurs when the backing lagoon overtops the berm in response to fluvial inflow (Parkinson and Stretch, 2007; Behrens et al., 2009) or ocean wave overtopping (Hart, 2009). In practice, many IOCE are artificially opened before a natural opening threshold is reached to alleviate flooding of property surrounding the lagoon (Haines and Thom, 2007).

During an opening, water outflow from the lagoon dominates sediment transport and the channel adjusts to the predominantly seaward direction of sediment movement (Stretch and Parkinson, 2006). Once the hydraulic head lessens, ocean waves become a main control on entrance morphodynamics and sediment is again reworked landward (Morris and Turner, 2010). Short waves (i.e. gravity frequency) are dominant, with entrance closure occurring through vertical accretion of the berm or longshore progradation of spits at the mouth (Ranasinghe and Pattiaratchi, 2003). While gravity

waves dominate sediment transport at the entrance (Gonzalez-Villanueva et al., 2017), infragravity (IG) frequency waves have been identified within IOCE basins while the entrance remains open (Dodet et el., 2013; Bertin and Olabarrieta, 2016; Williams and Stacey, 2016; Bertin et al., 2019; Mendes et al., 2019).

IG waves are fluctuations in surface water level with periods of 30 secs to 5 mins (Munk, 1951). IG waves are suggested to occur in IOCE because the estuary mouth acts as a low-pass filter that removes gravity-wave energy via breaking and dissipation but allows the uncoupling of IG energy (Harvey et al., 2016; Bertin et al., 2018; Melito et al., 2018). Waves at IG frequencies can then propagate upstream and into the lagoon (Bertin and Olabarrieta, 2016). The offshore tidal elevation, wave height, and nearshore sea level are identified as controls on IG wave energy within estuary basins (Williams and Stacey, 2016). In shallow estuaries, blocking of the IG waves can occur during opposing ebb-tidal currents and IG waves are of higher magnitude during flood tides (Dodet et al., 2013; Mendes et al., 2019). The presence of long period waves in the basin is important in modulating sediment transport and can directly contribute to entrance closure (Melito et al., 2018). For example, Bertin et al., (2019) observed IG waves to increase the instantaneous landward sand flux by two orders of magnitude at Albufeira Lagoon, Portugal.

In this study, we investigate the role of IOCE entrance morphology on long period wave attenuation within the estuarine lagoon. Changes in entrance morphology were monitored alongside a continuous record of basin water levels after three artificial openings at IOCE in Victoria, Australia. As a pilot study, the aim was to broadly quantify all long period waves within the lagoon and their association with entrance

morphology rather than focus on a specific energy band. We relate changes in IG wave frequency and magnitude to variability in both the offshore marine conditions and morphological change at the mouth. Understanding the controls on long period waves within the lagoon has implications for predicting sedimentation rates (Bertin et al., 2019), in-basin fine sediment transport (Talke and Stacey, 2003), and water column mixing (Williams, 2014).

2.0 Regional setting

The study was conducted at two IOCE on the west Victorian coast: the Aire (38.76 °S, 143.51 °E) and Anglesea River (38.46 °S, 144.90 °E) estuaries (Figure 1a-c). The open coast of west Victoria, Australia, is microtidal with mixed semidiurnal tides and a spring tidal range of 0.90-1.50 m (Bird, 1993). The coast is influenced by high-energy south-westerly swells with peak wave heights occurring during the Austral winter (Hughes and Heap, 2010). Coastal Victoria has a temperate climate with rainfall and river discharge being both seasonally and interannually variable (Hughes and James, 1989). Rivers draining coastal catchments experience peak flows during winter and low flows in summer.

Two artificial openings were monitored at Aire River (20/03/2014 and 10/05/2014) and one was monitored at Anglesea (14/02/2014) (Figure 1d-f). The Aire has a catchment area of 250 km^2 and length of 6.70 km. Mean annual rainfall is 895 mm/year and mean daily discharge is 0.82 m^3/s^{-1}. Mean offshore significant wave height (H_s) is 3.38 m and peak wave period (T_p) 13.25 secs (McSweeney, 2020). Anglesea has a catchment area of 125 km^2 and length of 3.50 km. Mean annual rainfall is 635 mm/year and at the time of this study the estuary had a constant daily discharge of 0.05 m^3/s^{-1} due to

discharge from the upstream Alcoa coal plant (Sharley et al., 2012). Mean offshore H_s is 2.54 m and T_p 13.22 secs (McSweeney, 2020).

3.0 Methods

Estuary entrance morphology was measured by repetitive topographic surveys using a Real Time Kinematic (RTK) GPS on a single long profile and a fixed cross-section (at the berm position) (Figure 1b-c). Surveying commenced prior to channel excavation and extended until entrance closure. Surveys were referenced to permanent benchmarks established relative to Australian Height Datum (AHD). Outflow velocity was measured during the first few hours of opening, while the channel was wadeable, using an ADV mounted on a wading rod as per Burks (2009). Five measurements were taken in the centre of the cross-section each time and averaged.

Due to the absence of operational wave buoys, offshore wave data was hindcast at 3-hourly intervals from NOAA's WAVEWATCH III (WWIII) model v.3.14 on a global 30 arcminute grid. While WWIII is accepted as a reliable source of hindcast data (Browne et al., 2007) and shows good agreement with buoy data in Australia (Hemer and Church, 2007), the lack of buoy data remains a limitation. Gauged fluvial discharge was obtained for Aire River from the Department of Land, Water, and Planning stream monitoring network (site: 235219).

For each opening, the estuary water level was continuously logged and corrected to AHD. Pressure sensors (Solinist Levelogger 30001) were anchored to the channel bed at four sites: (1) the mouth, and then (2) 200-300 m, (3) 500 m, and (4) 1.20-1.80 km upstream, the last being in the central basin (Figure 1b-c). Placement was selected to

ensure sensors were far enough away from the extent of channel bed erosion and sufficiently deep to prevent exposure following drainage. Data was logged at 0.2 Hz (5 sec) to allow for maximum storage and to capture long-period wave fluctuations. A higher frequency sampling rate would be ideal to accurately capture IG waves however at the time of instrumentation our study was not specifically designed for this purpose. Therefore, we recognize that the sampling frequency is low, and in future studies will be increased to be more suitable for capturing IG waves. A barometric pressure logger was installed within a 2 km radius of all loggers.

Each water level time series was then split into hourly windows for spectral analysis with n=720 data points in each hour (Table 1). Data was corrected for variations in atmospheric pressure and de-trended as per Karimpour and Chen (2017). For the second opening of Aire River, only data from logger 2 was used as the site 1 logger was buried for ~30% of the opening and the site 3 logger was stolen (Figure 1b). Data during the period of high velocity outflow (>2 m/s) was omitted for both openings at Aire River (Table 1). These hours (n=14 at Aire 1 and n=18 at Aire 2) produced noisy spectral plots indicating potential fluctuations due to the highly turbulent flow in the channel.

Data was separated into frequency components by a fast Fourier transform using the OCEANLYZ Ocean Wave Analyzing Toolbox v.1.3 (Karimpour, 2014) in MATLAB R2019b. The parameters listed in Table 2 were output from spectral analysis.

After all hourly IG wave bulk parameters were extracted, they were checked for tidal modulation. A Doodson X0 filter was applied to the hourly data to remove the tidal

signal from the hourly time series in MATLAB R2019b using a script from Oliver (2020) (https://ecjoliver.weebly.com/code.html). The filter was applied to data only once the estuary had finished draining to maintain accuracy in carrying forward the signal extraction.

The IG wave parameters defined in Table 2 were extracted to correspond with the timing of morphological surveys. These variables were then tested for strength of correlation with the offshore H_s, T_p, tidal elevation, and entrance morphology (cross-sectional area and bed elevation at the berm position). These parameters were selected for comparison to IG wave properties as they are described to potentially impact on IG wave magnitude within estuary basins (Williams and Stacey, 2016; Bertin et al., 2019). A non-parametric Kendall's *tau_b* was used as data is not normally distributed and the sample size (n=37) was small. Data from logger site 2 was used for Aire River and site 1 was used at Anglesea River.

4.0 Results

4.1 Aire River opening 1

Aire River was artificially opened on 20/03/14 and remained open for 21 days. For the first two hours, outflow velocity was <2 m/s, reaching a maximum of 3.80 m/s six hours after opening (Figure 4a). The basin water level stopped decreasing ~20 hours after opening, coinciding with the channel reaching its maximum cross-sectional area (291 m^2) and minimum elevation at the former berm position (-0.25 m AHD) (Figure 2a; Figure 3a; Figure 4b;). From 22/03/14 onwards, the berm elevation progressively increased and cross-sectional area decreased (Figure 3a; Figure 4c-j). While the entrance was open, low height oscillations (up to 148 mm) in basin surface water

elevation were observed up to 1.80 km upstream. These waves occurred at peak frequencies (f_p) of 0.0415-0.0022 Hz (T_p 24-454 secs) and were dominated by waves in the IG band (Figure 2d-e). At all loggers, IG wave height (H_{m0}) was highest during the first two tidal cycles after drainage and when offshore H_s was >5 m on 04/04/14 (Figure 2c-e). IG wave H_{m0} and peak frequency (f_p) increased during high tides indicating tidal modulation (Figure 2a-e). Spatially, H_{m0} and f_p were consistently higher at sites closest to the mouth (Figure 2e).

At site 2 (Aire River), peak H_{m0} (140 mm) occurred on the second high tide following basin drainage on 21/03/14 (Figure 2d; 2f). This coincided with the channel having reached its maximum depth and cross-sectional area (Figure 3a). At this time, offshore H_s was 4.45 m and tidal elevation 1.02 m (Figure 2b-c). As the channel infilled, IG wave H_{m0} progressively decreased (Figure 2e; Figure 3a). By 22/03/14, the berm had accreted to near AHD with H_{m0} (101 mm) and PSD decreasing (Figure 2e-g; Figure 3a). From 27/03/14-01/04/14, offshore H_s remained <3 m and IG wave H_{m0} and f_p further decreased (Figure 2c-e). By 01/04/14 a subaerial spit had formed at the mouth (Figure 4d). On 02/04/14-05/04/14, offshore Hs increased to >4 m resulting in a large volume of sand being deposited at the mouth (Figure 4f-h). Despite the channel bed being >1 m above AHD, an increase in IG wave H_{m0} (106 mm) and f_p occurred during these more energetic wave conditions (Figure 2c-i; 2 h-i; Figure 3a). On 07/04/14, the channel had further infilled (Figure 3a; Figure 4i) and basin surface water level oscillations decreased in H_{m0} (Figure 2d). For logger site 2, T_p remained within the IG band for all periods of analysis (Figure 2e).

4.2 Aire River opening 2

Aire River was opened again on 10/05/14 and stayed open for 11 days. For two hours following opening, outflow velocity was <2 m/s, increasing to a maximum of 4 m/s six hours after opening. The estuary took 24 hours to cease draining and the maximum channel dimensions were reached at the same time (Figure 3b; Figure 5a). The resultant channel was deeper and larger than the first opening (Figure 3b; Figure 6). IG waves were again recorded in the basin and logger site 2 is interpreted for consistency.

During the opening, IG waves had f_p of 0.0324-0.0023 Hz (T_p 31-417 secs) (Figure 5d-i). Late during the drainage phase, gravity waves propagating up the channel were observed to be blocked by outflow in the thalweg but to move up the channel margins (Figure 7a-d). Waves were then recorded at IG frequencies within the basin with H_{m0} 20-25 mm (Figure 5d-i). The maximum H_{m0} (112 mm) occurred on the first high tide following drainage (Figure 5a-f). At this time, the channel dimensions were at a maximum, offshore H_s was 3.17 m, and the offshore tidal elevation 0.87 m (Figure 5b-c; Figure 3b). From 12/05/14 onwards, the channel infilled, and the berm accreted, while IG wave H_{m0} decreased on average (Figure 5d-g; Figure 6d-j). On 15/05/14, H_{m0} (98 mm) increased as offshore H_s (4.71 m), T_p (15.09 secs), and the open ocean tidal amplitude (1.22 m) all increased (Figure 5b-h). Corresponding with further infill of the channel and a decrease in offshore H_s, IG wave H_{m0} progressively decreased from 16/05/14 onwards until the entrance closed on 21/05/14 (Figure 5b-i). f_p remained within the IG band and became slightly less variable (Figure 5e). When closed, low height (H_{m0} 2-4 mm) IG waves were still registered in the basin (T_p 48 sec) (Figure 5d-e).

4.3 Anglesea River

Anglesea was artificially opened on 14/02/14 and remained open for 8 days. The maximum recorded outflow velocity was 2.20 m/s occurring 8 hours after opening. This opening differed from those at Aire River as the channel was long (110 m) and shallow and the estuary did not cease draining until several days after opening (Figure 8a). As a result, the channel bed did not reach its lowest elevation (+0.66 m AHD) and maximum area (6.95 m^2) until 18/02/14 and tidal oscillations did not occur in the basin (Figure 8a-e). IG waves were observed within the basin with the maximum H_{m0} and f_p being orders of magnitude lower than at Aire River (Figure 8c; 8f-h). On 19/02/14, offshore H_s increased to >2 m increasing IG wave H_{m0} to a maximum of 5.06 mm (Figure 8c-d). This period of high waves infilled the channel and raised the berm to +2.50 m AHD on 20/02/14 (Figure 8e). The entrance then closed on 21/02/14. While closed, low power, long period waves were still observed in the basin at similar magnitudes as when the basin was draining (Figure 8a-c).

4.4 Controls on IG wave frequency and magnitude

IG wave H_{m0} showed a strong positive correlation with the offshore H_s (r=0.660, p=<0.01) and channel cross-sectional area (r=0.542, p=<0.01) and a negative relationship with bed elevation (r=0.428, p=<0.01) (Table 3). IG wave T_p showed a negative correlation with the cross-sectional area (r=-0.500, p <0.01), and offshore H_s (r=-0.633, p=<0.01) and T_p (r=-0.428, p=<0.01) (Table 3). The offshore tidal elevation showed no statistically significant relationship with any IG wave parameters (Table 3).

The relationships between H_{m0}, T_p, and the channel cross-sectional area, berm elevation, and offshore H_s are presented in Figure 9a-f and support the correlations in

Table 3. These relationships are best represented by logarithmic trendlines with the maximum R^2 values being between the basin IG wave H_{m0} and the channel cross-sectional area (R^2=0.85) and basin IG wave H_{mo} and offshore H_s (R^2=0.74).

5.0 Discussion

5.1 IOCE entrance dynamics

The influence of entrance channel morphology on water level oscillations can be framed as a six-stage conceptual model (Table 4; Figure 10a-c). The model is based on field observations during this study, combined with evidence from literature. Each stage shows a different dominance of wave, fluvial, and tidal processes and consequentially different rates of channel infill or erosion.

The estuary is opened through a shallow channel and the drainage rate lags behind the channel expansion rate (stage 1) (Table 4) (Parkinson and Stretch, 2007; Wainwright and Baldock, 2015). Outflow velocity is <2m/s and sediment transport initiates in an offshore direction (Gordon, 1990; Haines, 2006). Once the headcut created at the seaward face of the berm propagates up to the lagoon, rates of channel expansion and estuary drainage increase (stage 2) (Figure 10a-c). Here the estuary is strongly dominated by fluvial processes and outflow is often supercritical with velocities of 2-5 m/s (Gordon, 1990; Haines, 2006). Late in stage 2, the channel reaches equilibrium dimensions (Stretch and Parkinson, 2006). As hydraulic head between the lagoon and the ocean falls, the estuary ceases draining.

Immediately after the estuary has ceased draining (stage 3), the channel remains close to its maximum dimensions which permits the propagation of waves and tides into the basin (Hanes et al., 2011). Here tidal energy is at a theoretical maximum

(Figure 10a-c; Table 4). If ebb-tidal currents weaken, deposition will commence with progressive berm building and channel infill (Figure 10a-c; Table 4). This may occur on the first high tide following opening if the ebb-tidal prism is small (Whitfield et al., 2008). Tidal signals become attenuated and the basin water level rises (stages 4-5). Eventually the entrance will close as hydraulic efficiency decreases (stage 6) (Table 4) (Hinwood and McLean, 2001; Battalio et al., 2007). If river flow increases, a temporary reset of the channel may occur with seaward erosion of sediment. Thus, the estuary can transition between these stages as a function of the relative energy balance between fluvial and marine processes.

5.2 IG waves within IOCE basins

In this study, water level oscillations in the IG frequency band were consistently observed within IOCE up to 1.80 km upstream of the mouth, being most prominent during high tides. The kilometre-scale distance of inland penetration into the basin has also been observed in IOCE in California (USA) (Williams, 2014) and Portugal (Bertin and Olabarrieta, 2016) at decimetre amplitudes. A limitation on this penetration is the rate of outflow, from ebbing tides or basin drainage, especially when velocities exceed >2 m/s (Dodet et al., 2013; Bertin et al., 2018). At our sites, IG waves were present during the late stages of basin drainage, yet at low H_{m0}, likely occurring when outflow velocity had decreased <2 m/s (Figure 10d). We attribute the IG signal to waves which track the margins of the entrance channel, away from the thalweg, to then propagate into the basin (Figure 7; supplementary material). These waves were observed to contribute to bank erosion by undercutting the toe of the channel (Figure 7c), and when in-channel wave setup occurred, waves saturated the banks to drive slaking (supplementary material). IG wave magnitude was consistently highest coinciding with

the channel reaching its maximum cross-sectional area and depth immediately after the basin had ceased draining (i.e. early in stage 3; Table 4).

5.2 Influence of entrance morphology

IOCE entrance morphology is constantly changing over rapid timescales in response to process variability at the mouth (Morris and Turner, 2010; Rich and Keller, 2013; Slinger, 2017). At our field sites, entrance morphology had the strongest influence on the magnitude of IG waves occurring in the estuarine lagoon. IG wave H_{m0} showed a strong positive correlation with the channel cross-sectional area and a negative correlation with the berm/bed elevation (Table 3). This means that as the channel infills and the berm accretes, IG wave magnitude decreases. The cross-sectional area consistently showed the strongest correlation with IG wave parameters as it represents not only the depth at the mouth but the total area which waves can propagate through. When the entrance channel is long (>100 m) and the channel bed at the mouth is above AHD (i.e. as at Anglesea) this largely inhibits the influence of tides and long-period waves into IOCE basins.

In relation to the conceptual model of the opening sequence, IG wave magnitude is at a maximum early during stage 3 when the channel dimensions are largest and outflow velocity (and its potential blocking effect) has decreased (Figure 10d). When the mouth infills and the berm accretes above mean sea level, by the commencement of stage 5 IG wave H_{m0} decreases substantially in the absence of high offshore waves. When closed, in stage 6, low power IG waves can still influence the basin (e.g. Figure 5d-e) meaning the estuary is not wholly “disconnected” from the ocean. This may influence mixing processes and salinity within the seaward portion of the lagoon.

5.4 Influence of offshore marine conditions

Previous work has identified that more energetic ocean wave conditions correspond to an increased wave climate within IOCE (Bertin and Olabarrieta, 2016; Williams and Stacey, 2016; Melito et al., 2018). This is consistent with our findings (Table 3). Increases in offshore H_s most strongly translated to increases in IG magnitude when the channel bed at the mouth remained below AHD (stages 3-4). Despite this, our data shows that even when berms fronting ICOE are above AHD (i.e. stages 5-6), high (>4 m) offshore waves can still drive a temporary increase in IG wave H_{m0}. This was observed at the Aire River on 03/04 (Figure 2d) and 15/05 (Figure 5d). These increases in H_{m0} are event driven and controlled by the magnitude and duration of more energetic offshore wave conditions. Prior work states that a higher tidal elevation increases IG wave magnitude as the estuary becomes more connected to the nearshore (Williams and Stacey, 2016; Bertin et al., 2018). Our data show a similar tidal modulation where IG wave H_{m0} increased during high tides - especially while the entrance cross-sectional area remained large. When combined with high offshore H_s, this has the potential to deliver the maximum amount of energy from the offshore marine environment. While the offshore tidal elevation did not show a strong correlation with IG properties at our sites, this may be due to the lower tidal range compared to estuaries in previous studies (e.g. 2.5 m; Bertin et al., 2019).

In regions with an energetic wave climate, IG wave velocities can be higher than tidal velocities and act as a dominant mechanism of channel infill (Williams, 2014). While particle scale sediment tracking was outside the scope of this study, Dodet et al., (2013); Bertin and Olabarrieta (2016) report that the presence of IG waves can increase sand transport into an estuary by up to 20% during flood tides. IG waves also

cause bursts of kinetic energy which contributes to mixing of the water column (Williams, 2014). As many IOCE become stratified, IG motions are likely to play a main role in reducing salinity stratification. As the influence of these waves was recorded 1.80 km upstream at our sites, they are potentially an important driver of mixing for the whole lagoon

5.4 Intra basin changes in IG waves

Our observations show that H_{m0} and f_p decrease in a non-linear fashion with distance upstream from the mouth (Figure 2d-e). This is attributed to the loss of energy via dissipation into the basin. An example of this is presented in Figure 11. A shift in the spectra towards the dominance of lower frequency waves is evident and the higher frequency peaks observed near the mouth are lost upstream. Here the wavelength is becoming longer with distance away from the wave source. This process is analogous to changes in waves moving across a coral reef where swell waves dissipate on the reef crest causing IG waves to dominate at progressively lower frequencies towards the lagoon (Lowe et al., 2005; Pomeroy et al., 2012).

6.0 Conclusion

Wave-current interactions play a main role in the hydrodynamics and sediment transport of IOCE. Our field observations show that water level oscillations in the IG band are a persistent feature in IOCE basins and may be the norm rather than the exception in these systems. We have linked changes in IG wave frequency and magnitude to variability in estuary entrance morphology and offshore marine conditions during an opening. IG wave H_{m0} is highest when the cross-sectional area is largest and/or with large offshore wave heights. This generally occurs with the first

few high tides following estuary drainage (i.e. stage 3; Table 4). Changes in the magnitude and frequency of IG waves exemplify the role of entrance morphology in controlling internal conditions within the lagoon. Prior work by Bertin et al., (2019) report that individual IG waves can increase the sand flux rate by at least 2 orders of magnitude. While we could not directly quantify the role of IG in sediment transport, basin infill, and, erosion, we do identify and quantify the properties of the IG waves in our study basins.

In this study IG waves were captured serendipitously within IOCE as part of a larger field campaign. Future work will focus on instrumenting IOCE to gain high resolution data to quantify the precise (a) relationship with nearshore wave conditions; (b) intra-basin changes in IG wave properties (including between IOCE with different basin morphologies); and (c) influence on sediment transport.

7.0 Acknowledgements

This research received no specific funding. Corangamite Catchment Management Authority and Parks Victoria are thanked for letting us know of the timing of artificial openings. The authors declare no conflict of interest.

8.0 Data Availability Statement

The data that support the findings of this study are available from the corresponding author upon reasonable request.

9.0 References

Battalio, B., Danmeier, D. and Williams, P., 2007. Predicting closure and breaching frequencies of small tidal inlets–a quantified conceptual model. In Coastal Engineering 2006: (In 5 Volumes) (pp. 3937-3949).

Behrens, D.K., Bombardelli, F.A., Largier, J.L. and Twohy, E., 2009. Characterization of time and spatial scales of a migrating rivermouth. Geophysical Research Letters, 36(9).

Behrens, D.K., Bombardelli, F.A., Largier, J.L. and Twohy, E., 2013. Episodic closure of the tidal inlet at the mouth of the Russian River—A small bar-built estuary in California. Geomorphology, 189, pp.66-80.

Bertin, X. and Olabarrieta, M., 2016. Relevance of infragravity waves in a wave-dominated inlet. Journal of Geophysical Research: Oceans, 121(8), pp.5418-5435.

Bertin, X., de Bakker, A., Van Dongeren, A., Coco, G., Andre, G., Ardhuin, F., Bonneton, P., Bouchette, F., Castelle, B., Crawford, W.C. and Davidson, M., 2018. Infragravity waves: From driving mechanisms to impacts. Earth-Science Reviews, 177, pp.774-799.

Bertin, X., Mendes, D., Martins, K., Fortunato, A.B. and Lavaud, L., 2019. The closure of a shallow tidal inlet promoted by infragravity waves. Geophysical Research Letters, 46(12), pp.6804-6810.

Bird, E.C.F., 1993. The coast of Victoria: the shaping of scenery. Melbourne Univ Press. Melbourne, Australia.

Burks, T., 2009. Standard Operating Procedure for Measuring Stream Discharge Using the Son-Tek FlowTracker Hand held ADV. Environmental Assessment Program, Washington State Department of Ecology. Document available at: http://www.ecy.wa.gov/programs/eap/quality.html

Browne, M., Castelle, B., Strauss, D., Tomlinson, R., Blumenstein, M. and Lane, C., 2007. Near-shore swell estimation from a global wind-wave model: Spectral process, linear, and artificial neural network models. Coastal Engineering, 54(5), pp.445-460.

Cooper, J.A.G., 2002. The role of extreme floods in estuary-coastal behaviour: contrasts between river-and tide-dominated microtidal estuaries. Sedimentary Geology, 150(1-2), pp.123-137.

Dodet, G., Bertin, X., Bruneau, N., Fortunato, A.B., Nahon, A. and Roland, A., 2013. Wave-current interactions in a wave-dominated tidal inlet. Journal of Geophysical Research: Oceans, 118(3), pp.1587-1605.

González-Villanueva, R., Pérez-Arlucea, M. and Costas, S., 2017. Lagoon water-level oscillations driven by rainfall and wave climate. Coastal Engineering, 130, pp.34-45.

Gordon, A.D., 1990. Coastal lagoon entrance dynamics. In Coastal Engineering 1990 (pp. 2880-2893).

Griffiths, S.P., 2001. Factors influencing fish composition in an Australian intermittently open estuary. Is stability salinity-dependent? Estuarine, Coastal and Shelf Science, 52(6), pp.739-751.

Haines, P.E., 2006. Physical and chemical behaviour and management of Intermittently Closed and Open Lakes and Lagoons (ICOLLs) in NSW. Griffith University. PhD thesis. https://research-repository.griffith.edu.au/bitstream/handle/10072/367425/Haines_2006_01Thesis.pdf?sequence=1

Haines, P.E. and Thom, B.G., 2007. Climate change impacts on entrance processes of intermittently open/closed coastal lagoons in New South Wales, Australia. Journal of Coastal Research, pp.242-246.

Hanes, D.M., Ward, K. and Erikson, L.H., 2011. Waves and tides responsible for the intermittent closure of the entrance of a small, sheltered tidal wetland at San Francisco, CA. Continental Shelf Research, 31(16), pp.1682-1687.

Hart, D.E., 2009. Morphodynamics of non-estuarine rivermouth lagoons on high-energy coasts. Journal of Coastal Research, 56(2), pp.1355-1359.

Harvey, M., Giddings, S.N. and Pawlak, G., 2016. Wave Induced Sediment Transport in a Bar-Built Estuary in Southern California, USA. Abstract for the 18th Physics of Estuaries and Coastal Seas Conference, 2016. https://diamweb.ewi.tudelft.nl/pecs2016/abstracts/MadeleineHarvey.pdf

Hemer, M.A., Church, J.A. and Hunter, J.R., 2007. Waves and climate change on the Australian coast. Journal of Coastal Research, pp.432-437.

Hinwood, J.B. and McLean, E.J., 2001. Monitoring and modelling tidal regime changes following inlet scour. Journal of Coastal Research, pp.449-458.

Hughes, J.M.R. and James, B., 1989. A hydrological regionalization of streams in Victoria, Australia, with implications for stream ecology. Marine and Freshwater Research, 40(3), pp.303-326.

Hughes, M.G. and Heap, A.D., 2010. National-scale wave energy resource assessment for Australia. Renewable Energy, 35(8), pp.1783-1791.

Karimpour, A., 2014. OCEANLYZ: Ocean Wave Analyzing Toolbox v.1.3. Downloaded from: http://www.arashkarimpour.com/oceanlyz.html

Karimpour, A. and Chen, Q., 2017. Wind wave analysis in depth limited water using OCEANLYZ, A MATLAB toolbox. Computers & Geosciences, 106, pp.181-189.

Lowe, R.J., Falter, J.L., Bandet, M.D., Pawlak, G., Atkinson, M.J., Monismith, S.G. and Koseff, J.R., 2005. Spectral wave dissipation over a barrier reef. Journal of Geophysical Research: Oceans, 110(C4).

McSweeney, S.L., Kennedy, D.M., Rutherfurd, I.D. and Stout, J.C., 2017. Intermittently Closed/Open Lakes and Lagoons: Their global distribution and boundary conditions. Geomorphology, 292, pp.142-152.

McSweeney, S.L., Kennedy, D.M. and Rutherfurd, I.D., 2018. The daily-scale entrance dynamics of intermittently open/closed estuaries. Earth Surface Processes and Landforms, 43(4), pp.791-807.

McSweeney, S.L., 2020. Temporal and spatial variability of the open coast wave climate of Victoria, Australia. Marine and Freshwater Research, 71(3), pp.394-413.

Melito, L., Postacchini, M., Sheremet, A., Calantoni, J., Zitti, G., Darvini, G. and Brocchini, M., 2018. Wave-Current Interactions and Infragravity Wave Propagation at a Microtidal Inlet. In Multidisciplinary Digital Publishing Institute Proceedings (Vol. 2, No. 11, p. 628).

Mendes, D., Fortunato, A.B., Bertin, X., Martins, K., Lavaud, L., Silva, A.N., Pires-Silva, A.A., Coulombier, T. and Pinto, J.P., 2019. Importance of infragravity waves in a wave-dominated inlet under storm conditions. Continental Shelf Research, p.104026.

Morris, B.D. and Turner, I.L., 2010. Morphodynamics of intermittently open–closed coastal lagoon entrances: new insights and a conceptual model. Marine Geology, 271(1-2), pp.55-66.

Munk, W.H., 1951. Origin and generation of waves, Proc. First Conf. on Coastal Eng., Long Beach, California, U.S.A.

Parkinson, M. and Stretch, D., 2007. Breaching timescales and peak outflows for perched, temporary open estuaries. Coastal engineering journal, 49(03), pp.267-290.

Ranasinghe, R. and Pattiaratchi, C., 1999. The seasonal closure of tidal inlets: Wilson Inlet—a case study. Coastal Engineering, 37(1), pp.37-56.

Pomeroy, A., Lowe, R., Symonds, G., Van Dongeren, A. and Moore, C., 2012. The dynamics of infragravity wave transformation over a fringing reef. Journal of Geophysical Research: Oceans, 117(C11).

Ranasinghe, R. and Pattiaratchi, C., 2003. The seasonal closure of tidal inlets: causes and effects. Coastal engineering journal, 45(04), pp.601-627.

Rich, A. and Keller, E.A., 2013. A hydrologic and geomorphic model of estuary breaching and closure. Geomorphology, 191, pp.64-74.

Roy, P.S., Williams, R.J., Jones, A.R., Yassini, I., Gibbs, P.J., Coates, B., West, R.J., Scanes, P.R., Hudson, J.P. and Nichol, S., 2001. Structure and function of south-east Australian estuaries. Estuarine, Coastal and Shelf Science, 53(3), pp.351-384.

Sharley, D., Amos, C. and Pettigrove, V., 2012. Factors Affecting the Ecology of the Anglesea River. Report for Corangamite Catchment Management Authority: Victoria, Australia. http://www.ccmaknowledgebase.vic.gov.au/resources/Factors_affecting_the_ecology_of_the_Anglesea_River.pdf

Slinger, J.H., 2017. Hydro-morphological modelling of small, wave-dominated estuaries. Estuarine, Coastal and Shelf Science, 198, pp.583-596.

Stretch, D. and Parkinson, M., 2006. The breaching of sand barriers at perched, temporary open/closed estuaries—A model study. Coastal Engineering Journal, 48(01), pp.13-30.

Talke, S.A. and Stacey, M.T., 2003. The influence of oceanic swell on flows over an estuarine intertidal mudflat in San Francisco Bay. Estuarine, Coastal and Shelf Science, 58(3), pp.541-554.

Wainwright, D.J. and Baldock, T.E., 2015. Measurement and modelling of an artificial coastal lagoon breach. Coastal Engineering, 101, pp.1-16.

Whitfield, A.K., Adams, J.B., Bate, G.C., Bezuidenhout, K., Bornman, T.G., Cowley, P.D., Froneman, P.W., Gama, P.T., James, N.C., Mackenzie, B. and Riddin, T., 2008. A multidisciplinary study of a small, temporarily open/closed South African estuary, with particular emphasis on the influence of mouth state on the ecology of the system. African Journal of Marine Science, 30(3), pp.453-473.

Williams, M., 2014. Hydrodynamics and salt dispersion in intermittently closed bar-built estuaries (Doctoral dissertation, UC Berkeley). Available online: https://digitalassets.lib.berkeley.edu/etd/ucb/text/Williams_berkeley_0028E_14663.pdf

Williams, M.E. and Stacey, M.T., 2016. Tidally discontinuous ocean forcing in bar-built estuaries: The interaction of tides, infragravity motions, and frictional control. Journal of Geophysical Research: Oceans, 121(1), pp.571-585.

Table 1. Number of hourly windows of water level data analysed and omitted from spectral analysis and the total duration of each water level dataset.

Opening	Number of hourly windows	Hours omitted	Data duration (days)
Aire River 1	442	14	19.08
Aire River 2	312	18	13.17
Anglesea River	211	0	8.79

Table 2. Variables output from spectral analysis of the basin water level time series.

Variable	Description	Unit
PSD	Water surface elevation power spectral density	m^2s
f	Frequency	Hz
H_{m0}	Zero moment wave height	mm
T_{m01}	Wave period from moments 0 and 1	sec
T_{m02}	Wave period from moments 0 and 2	sec
T_p	Peak wave period	sec
f_p	Peak wave frequency	Hz

Table 3. Correlations between IG wave parameters extracted from spectral analysis and the corresponding channel cross-sectional area and bed elevation, and offshore tidal evaluation, H_s, and T_p. ** indicates correlation is significant at the 0.01 level (2-tailed) and * indicates correlation is significant at the 0.05 level (2-tailed).

	Kendall's tau_b	**Parameters from spectral analysis of basin water level data**				
		H^{m0}	**f_p**	**T_p**	**Tm_{01}**	**Tm_{02}**
Cross-sectional area	Correlation coefficient	**0.542****	**0.491****	**-0.500****	-0.130	-0.078
	Sig. (2-tailed)	**0.001**	**0.001**	**0.001**	0.257	0.496
Channel bed elevation	Correlation coefficient	**-0.428****	**-0.322****	**0.331****	-0.046	-0.075
	Sig. (2-tailed)	**0.000**	**0.005**	**0.004**	0.687	0.513
Offshore tidal elevation	Correlation coefficient	-0.016	-0.030	0.020	-0.020	0.022
	Sig. (2-tailed)	0.890	0.792	0.860	0.860	0.850
Offshore H_s	Correlation coefficient	**0.660****	**0.624****	**-0.633****	-0.286*	-0.242*
	Sig. (2-tailed)	**0.000**	**0.000**	**0.000**	0.012	0.033
Offshore T_p	Correlation coefficient	**0.393****	**0.413****	**-0.428****	-0.135	-0.044
	Sig. (2-tailed)	**0.001**	**0.000**	**0.000**	0.237	0.696

Table 4. Typical duration, dominant energy, and description of each stage in the sequence of IOCE opening/closure. The six stages correspond with Figure 10a-d. MSL refers to mean sea level (i.e. AHD for our sites).

Stage	Duration	Energy	Channel morphology	Basin hydrodynamics
1: Pilot channel	1-2 hrs	Fluvial	Creation of a shallow (<1 m deep), narrow (2-5 m) channel. A headcut is formed at the seaward edge of the berm.	An initial connection to ocean is formed. Slow basin drainage which lags channel expansion. Outflow velocity is <2 m/s.
2: Rapid expansion	6-36 hrs	Fluvial	Headcut reaches the basin. Rapid incision and widening. Berm eroded to below MSL. Antidunes present on bed.	Period of the most rapid drainage. Outflow velocity >2 m/s becoming supercritical and with standing waves.
3: Peak tidal influence	Tidal cycle-weeks	Tidal	Channel incision/expansion ceases. Channel bed is at or below MSL. Bidirectional bedforms are present due to tidal exchange.	Estuary basin stops draining. Outflow is no longer supercritical. Tidal signals are registered in basin if bed depth at mouth is below MSL.
4: Sub-aqueous berm accretion	Days-weeks	Wave	Subaqueous spit/berm may form at or near MSL. Most deposition in the seaward 50 m of channel. Channel cross-sectional area decreases.	Tides become highly dampened and attenuated in basin vs open ocean. Water level begins to rise in the estuary basin on average.
5: Sub-aerial berm accretion	Days-weeks	Wave	Berm elevation above MSL. The entrance may close temporarily at low tides. Accretion extends to lagoon. Decrease in channel area.	Loss of tidal signals except at high tides. Wave overwash is likely to influence basin. A progressive increase in water level in the estuary basin.
6: Entrance closure	Days-years	Wave	Berm now fully separates the estuary from ocean for longer than one tidal cycle. Infill of channel extends landward of berm crest and into lagoon.	Estuary water level continues to rise and may become perched above MSL. Wave overwash at high tide moves water/sediment landward.

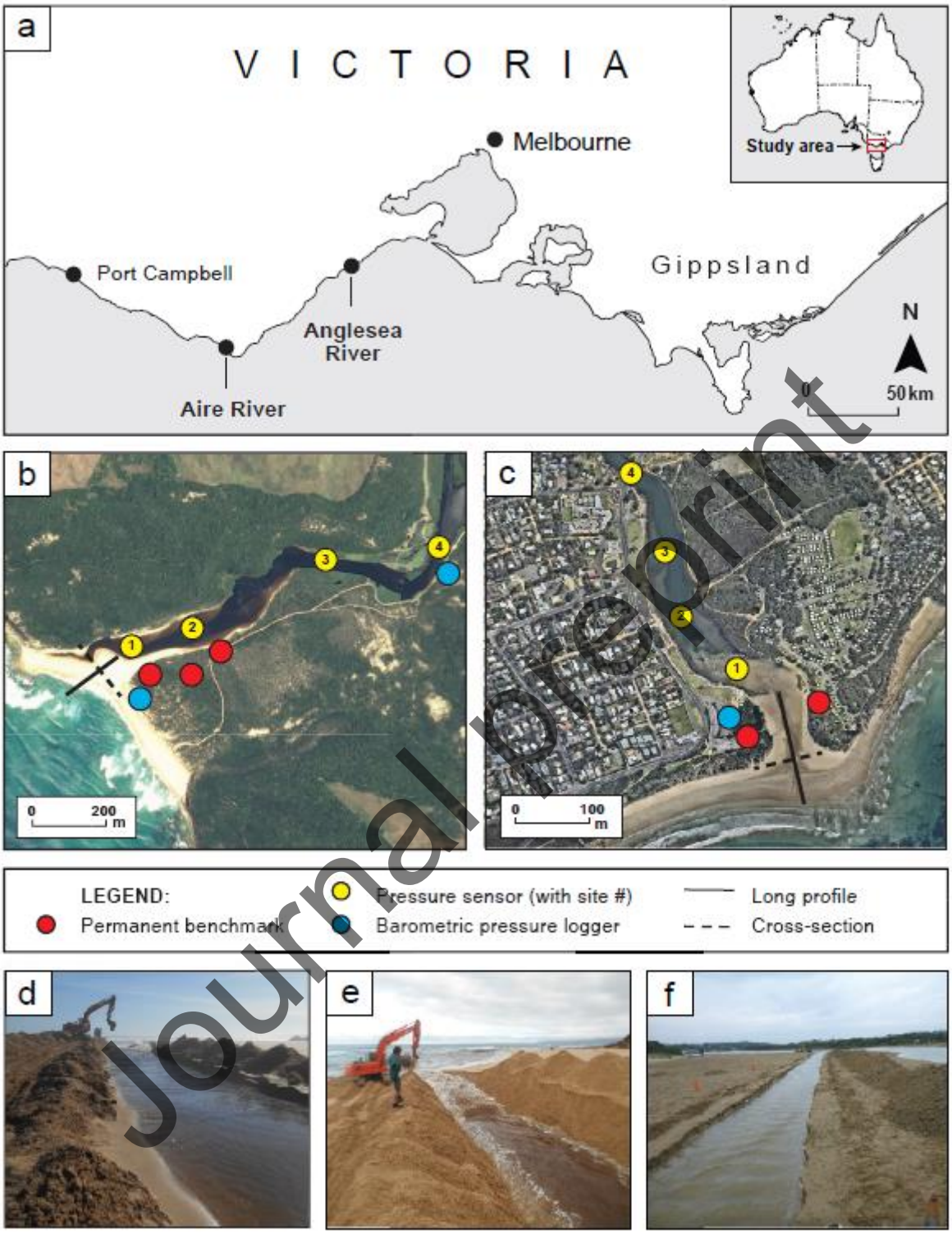

Figure 1a-f. (a) Location of study sites; field setup at the (b) Aire and (c) Anglesea River estuaries; (d) first artificial opening of Aire River 20/03/14 (looking seaward); (e) second opening of Aire River 11/05/14 (looking seaward); and (f) artificial opening of Anglesea River 14/02/14 (looking towards lagoon). All images taken 1-2 hours after channel excavation had commenced.

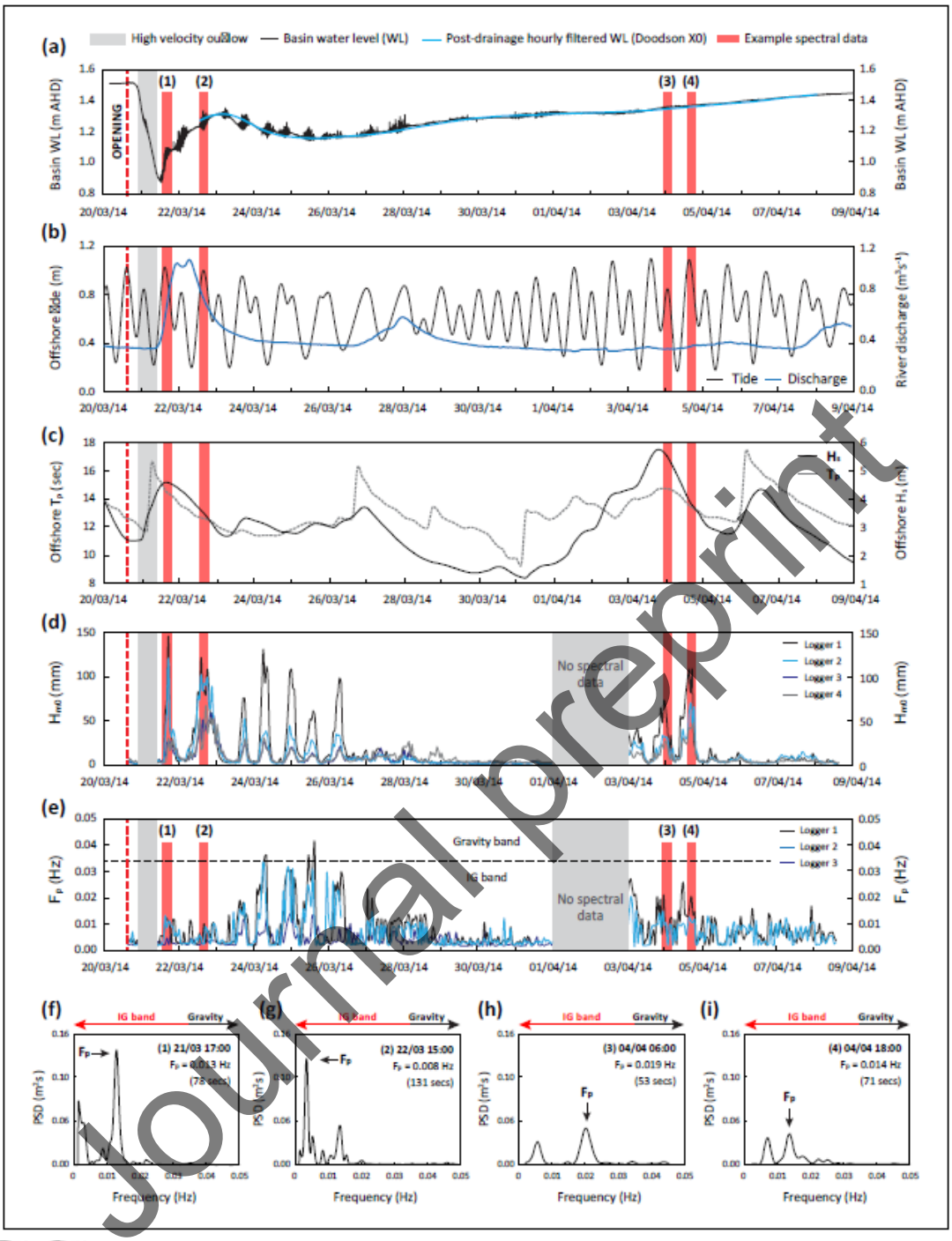

Figure 2a-i. (a) Basin water level time series during first artificial opening of Aire River (plotted every 2 mins for presentation) and hourly water level time series with tidal signal removed via a Doodson X0 filter. The grey box shows the period of high velocity outflow omitted fom spectral analysis. Red bands show data extracted for example spectral plots (f-i); (b) offshore tidal elevation and upstream fluvial discharge; (c) offshore H_s and T_p; (d) basin IG wave H_{m0} and (e) f_p (logger 4 is omitted here for presentation); and (f-i) example spectral plots for periods of interest using 1-hour windows of data from logger 2.

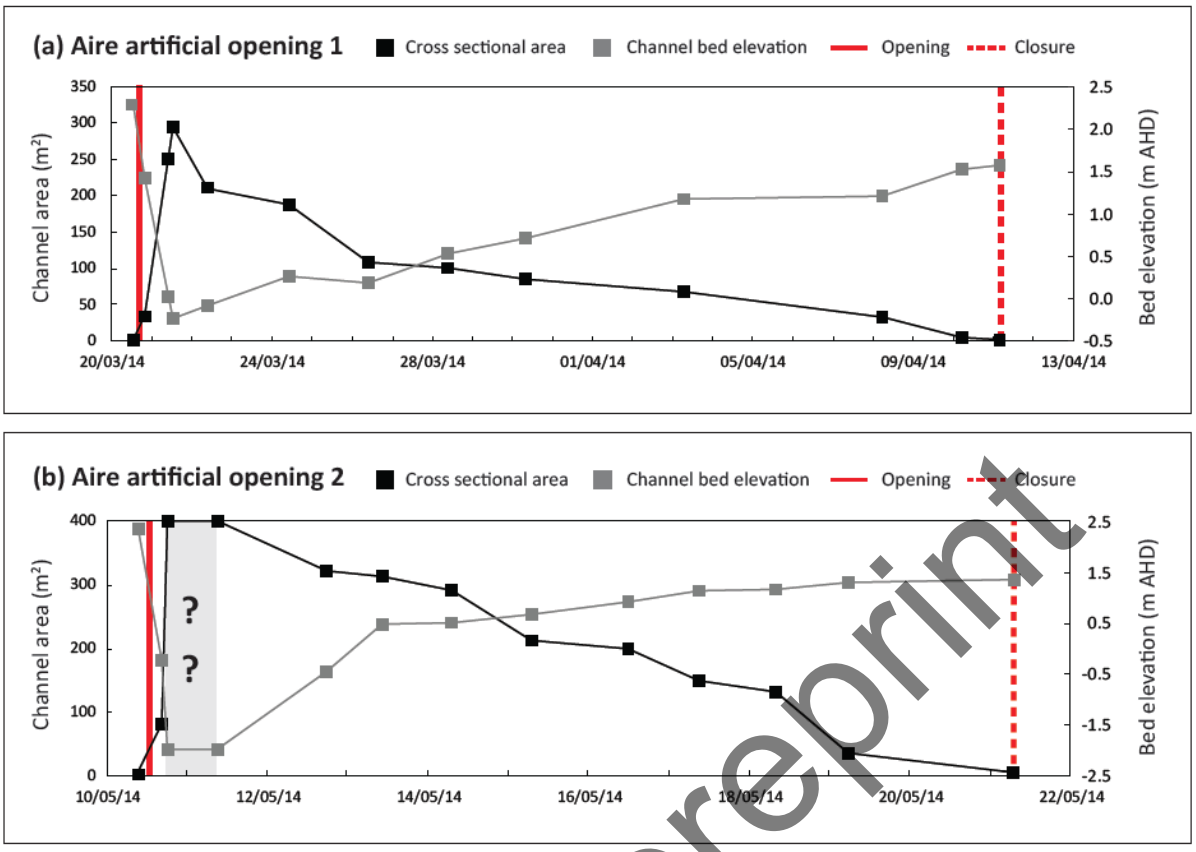

Figure 3a-b. Change in channel cross-sectional area and bed elevation at the berm position during (a) artificial opening 1, and (b) artificial opening 2 at Aire River. The grey box identifies a period of time where the estuary channel was too large and fast flowing to safely measure the morphology.

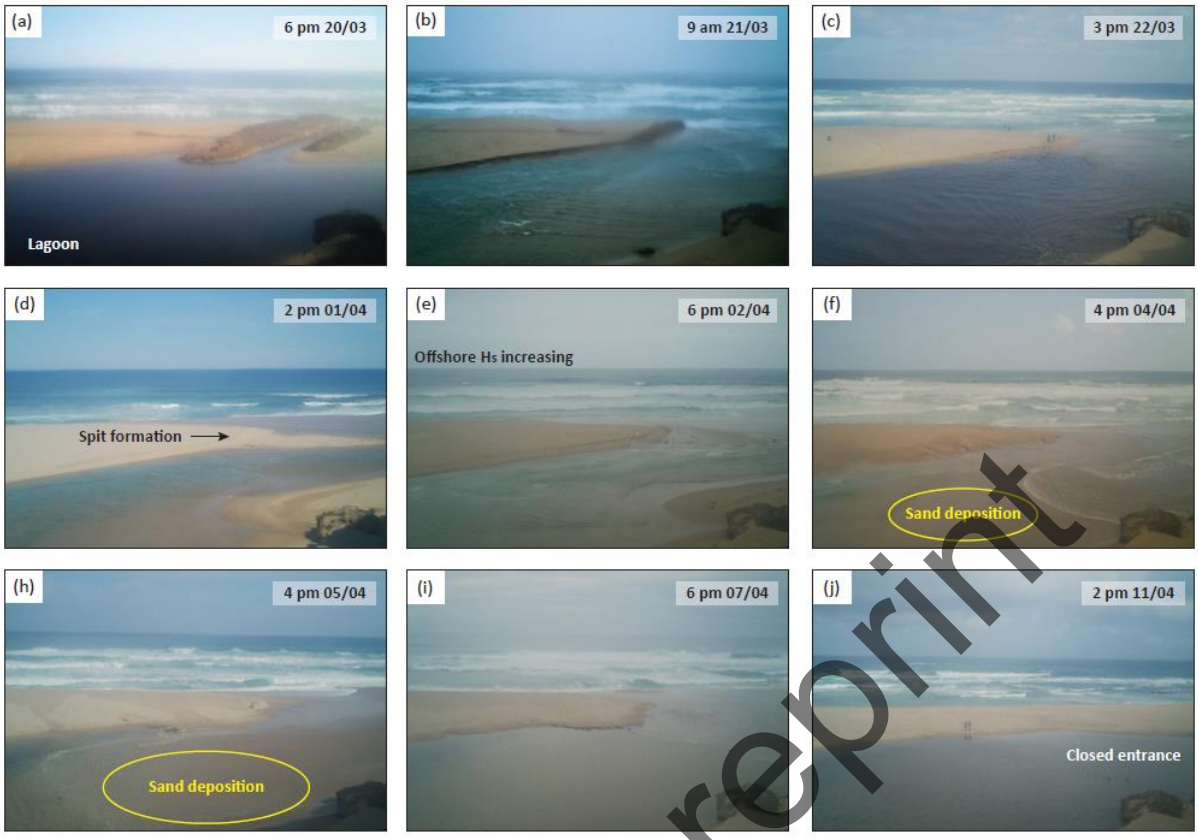

Figure 4a-j. Images of change in entrance morphology at Aire River following the first artificial opening. Images taken from a trail-cam fixed on an adjacent cliff. The time and date are annotated on each image.

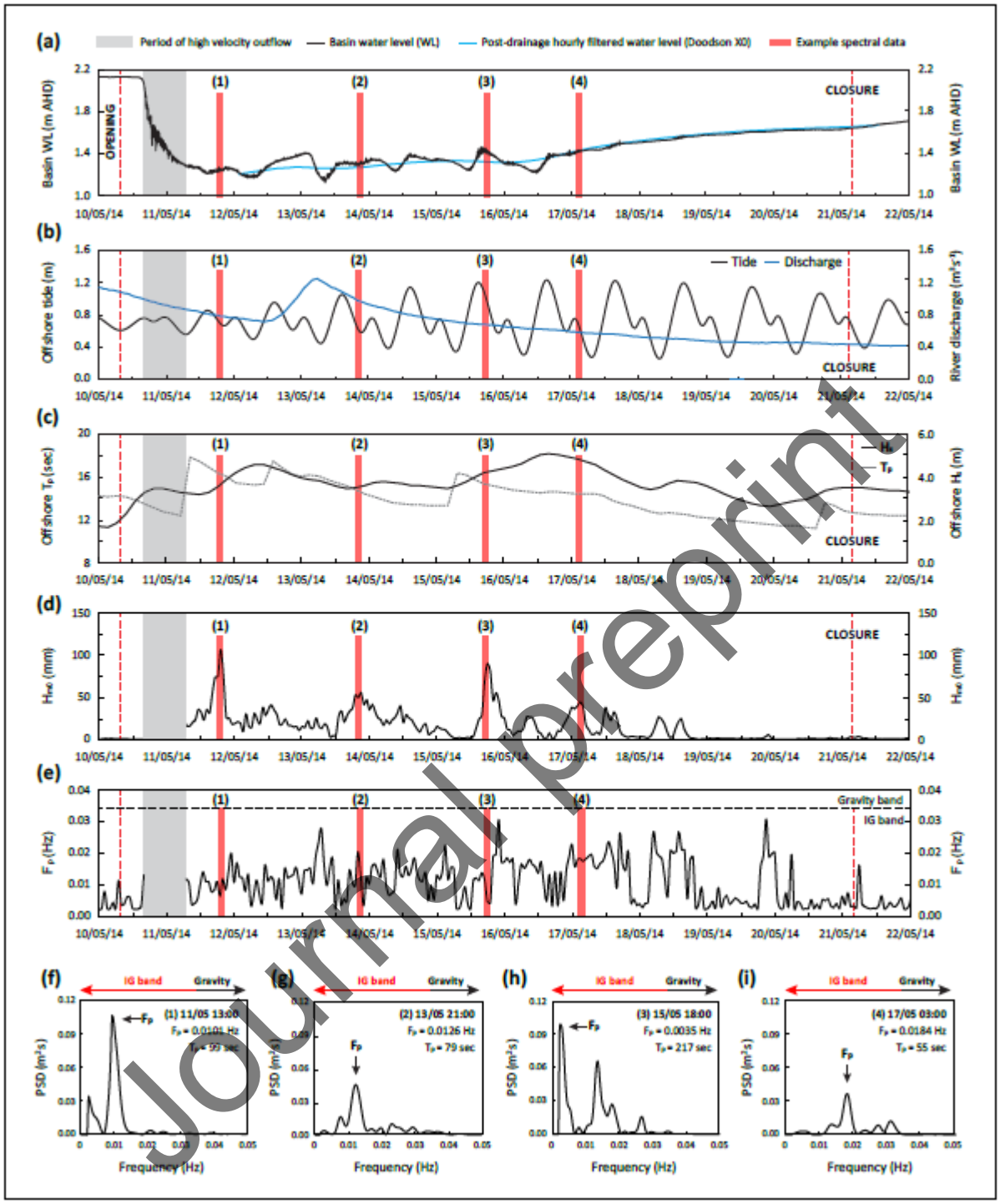

Figure 5a-i. (a) Basin water level time series during first artificial opening of Aire River (plotted every 2 mins for presentation) and hourly water level time series with tidal signal removed via a Doodson X0 filter. The grey box shows the period of high velocity outflow omitted fom spectral analysis. Red bands show data extracted for example spectral plots (f-i); (b) offshore tidal elevation and upstream fluvial discharge; (c) offshore H_s and T_p; (d) basin IG wave H_{m0} and (e) f_p (logger site 2); and (f-i) example spectral plots for periods of interest using 1-hour windows of data from logger 2.

Figure 6a-j. Images of change in entrance morphology at Aire River following the second artificial opening. Images taken from a trail-cam fixed on an adjacent cliff. The time and date are annotated on each image.

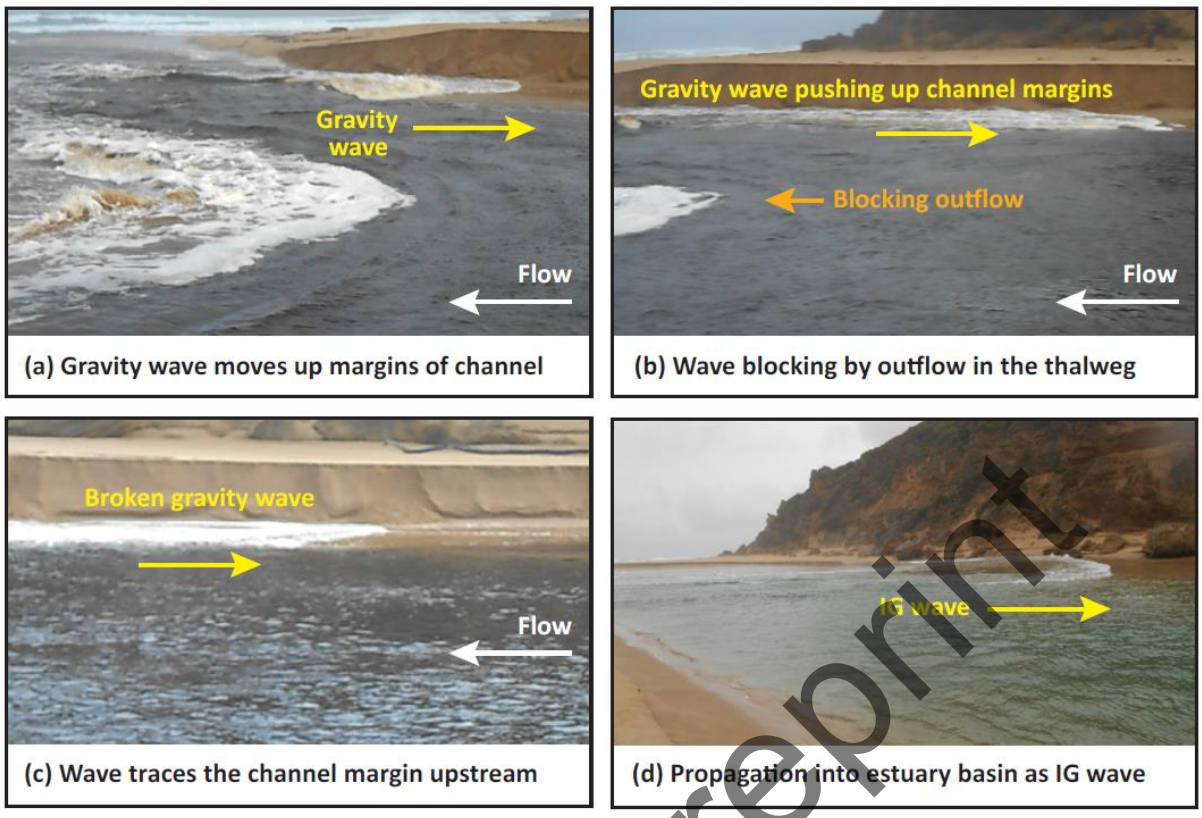

Figure 7a-d. Observed process of wave propagation into the estuary basin from the nearshore late in the drainage phase of ICOE. Here waves track the margins of the channel, away from the thalweg, to move into the lagoon. Note undercutting of the toe of the bank in (c).

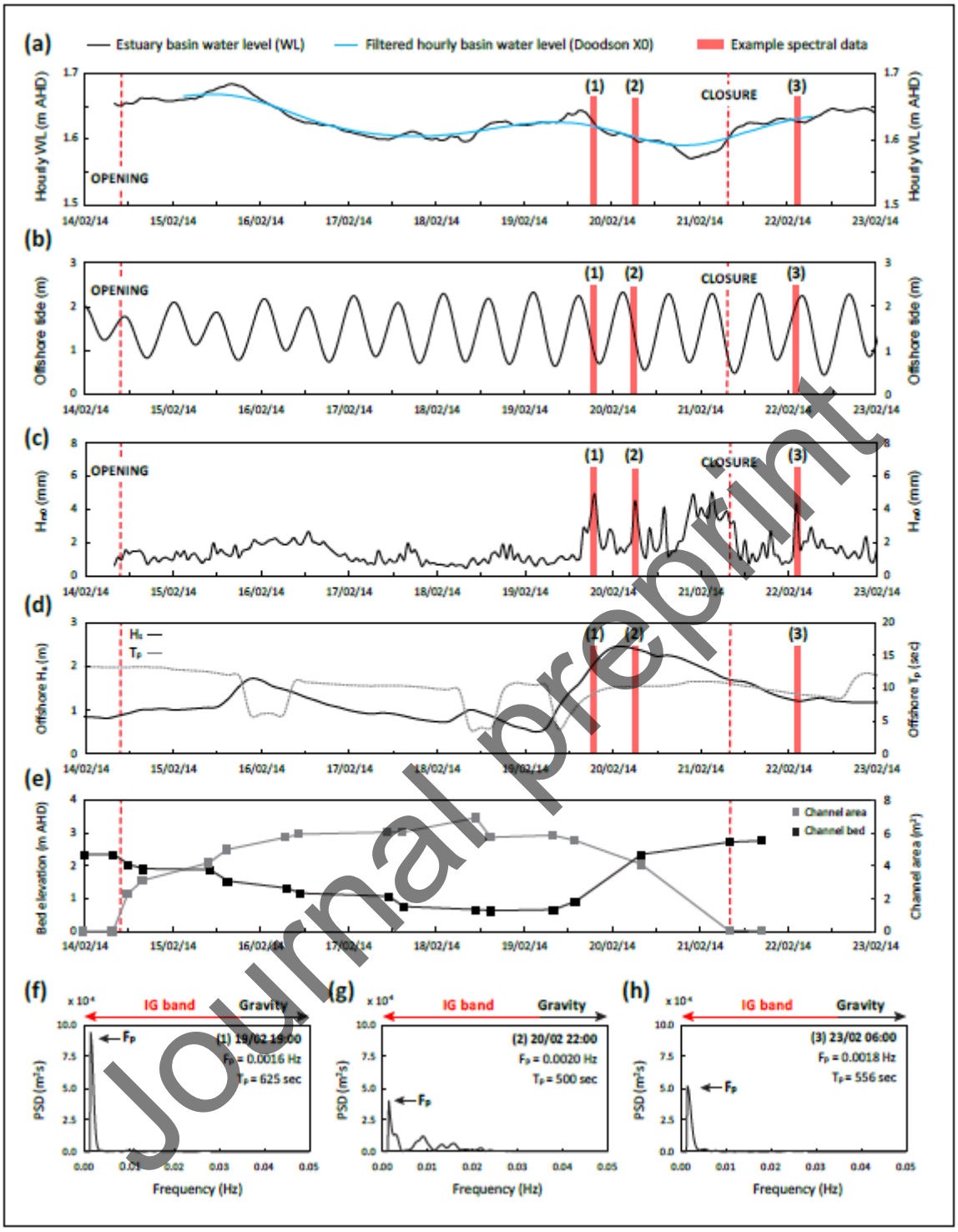

Figure 8a-h. (a) Water level time series during artificial opening of Anglesea River (plotted every 2 mins for presentation) and hourly water level time series with tidal signal removed via a Doodson X0 filter. Red bands show data extracted for example spectral plots (f-h); (b) offshore tidal elevation and (c) H_s and T_p; (d) basin IG wave H_{m0}; (e) cross-sectional area and bed elevation at the berm position; and (f-h) example spectral plots for periods of interest using 1-hour windows of data from logger 1.

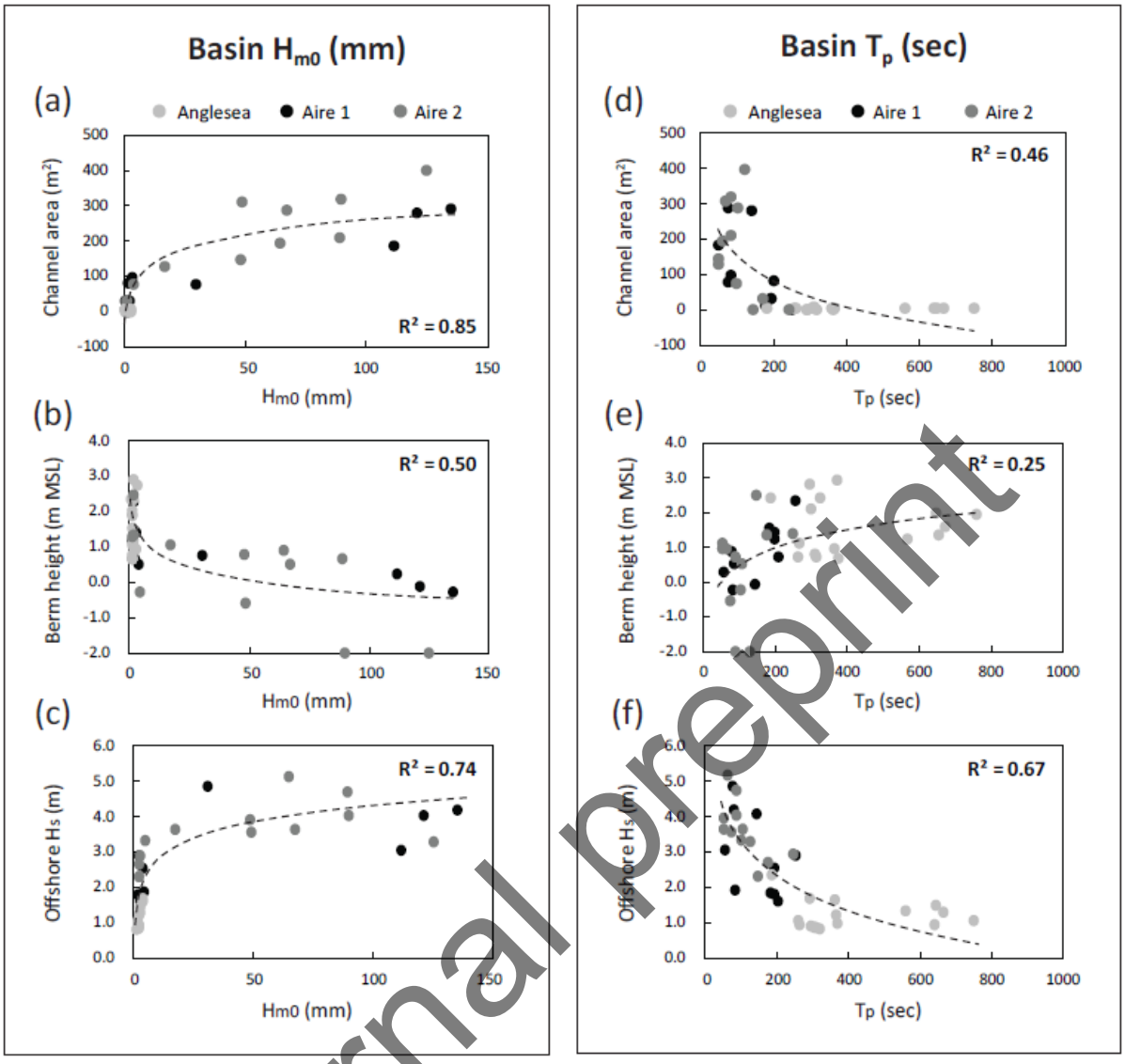

Figure 9a-f. Relationship between channel morphology, offshore H_s, and IG wave (a-c) H_{m0} and (d-f) T_p as extracted from each period of spectral analysis corresponding with the timing of morphological surveys at all IOCE sites.

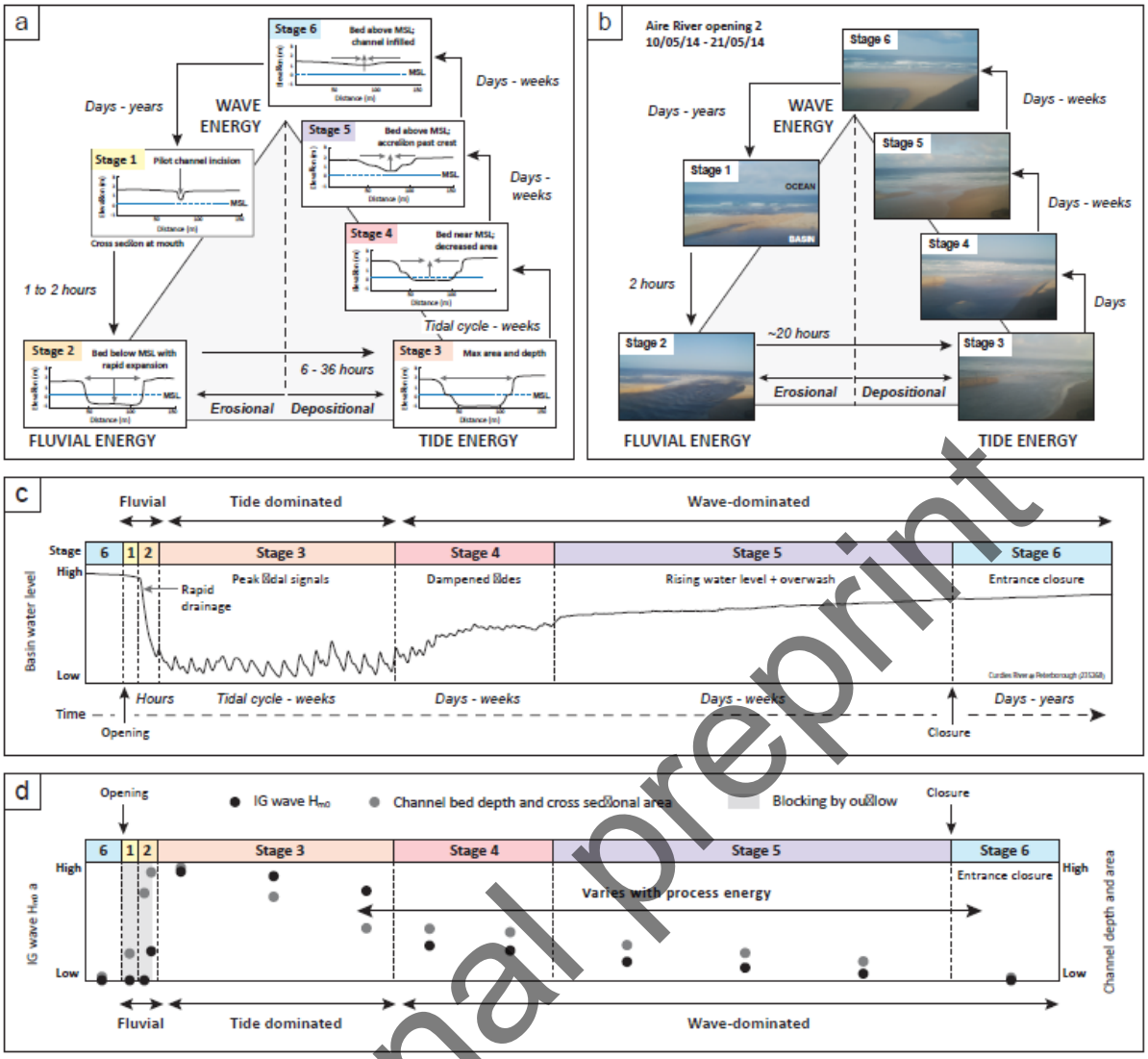

Figure 10a-d. Conceptual model of six-stages in the IOCE opening-closure sequence. Stages are defined in Table 4. (a) Changes in channel morphology with typical mouth cross-sections. Stage duration is annotated and the shift in energy dominance is represented by proximity to each point of the triangle; (b) supporting photos; (c) basin water level behaviour in each stage; and (d) idealised change in IG wave magnitude (represented by H_{m0}).

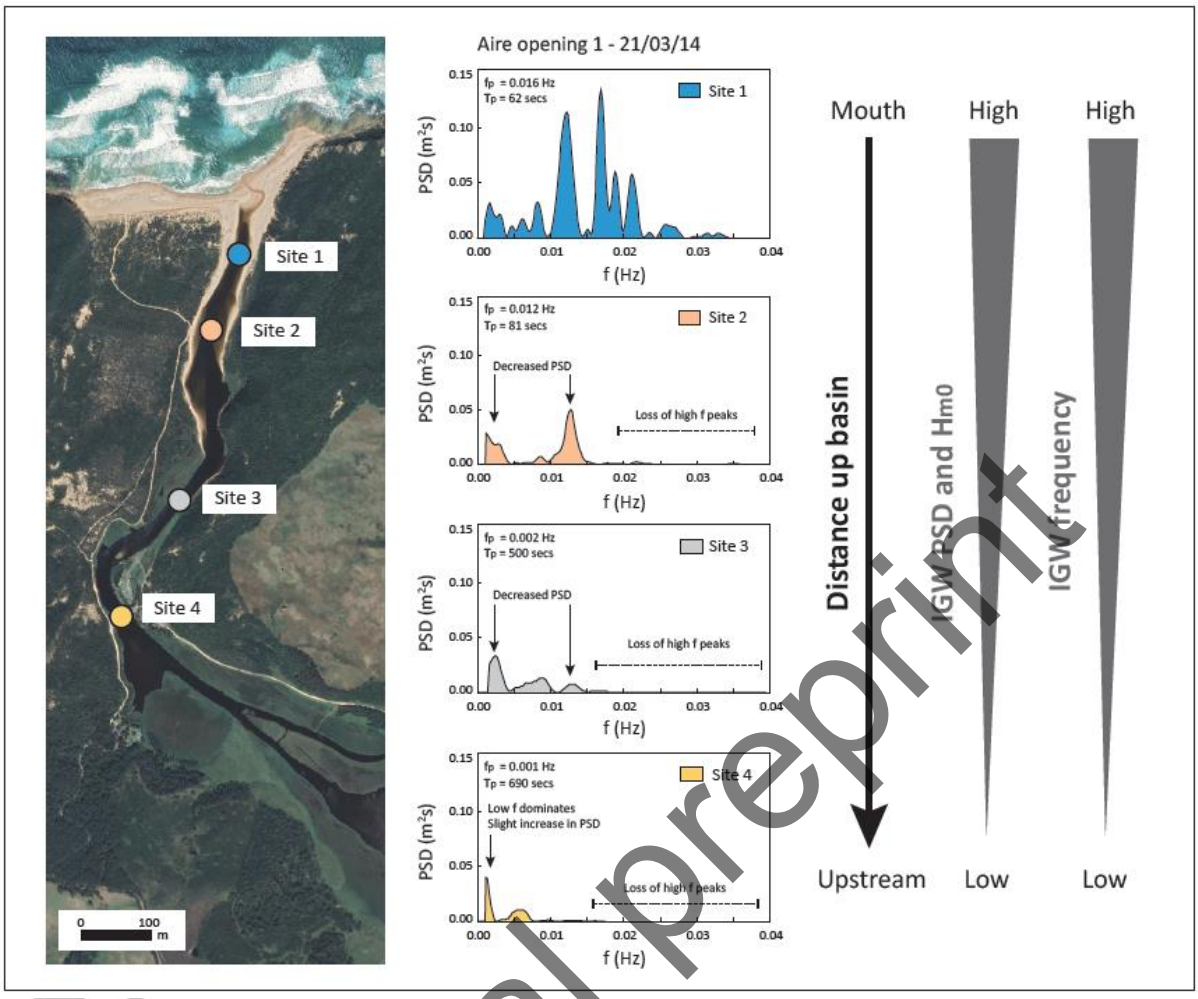

Figure 11. Intra basin changes in IG wave PSD, H_{m0}, and f_p with distance upstream of the mouth. Here PSD, H_{m0}, decrease and f_p decrease with a shift to lower frequency (longer-period) waves with distance away from the mouth. Data from Aire River (on 21/03/14) is used to exemplify this process.

Variability in infragravity wave processes during estuary artificial entrance openings.

Sarah L. McSweeney*, Justin C. Stout, and David M. Kennedy.

After an artificial estuary entrance opening, infragravity (IG) waves commonly are present within the estuarine lagoon. IG wave energy peaks when the channel dimensions are largest and immediately after the basin has ceased draining (stage 3). As the entrance infills (stages 4-6), IG wave magnitude progressively decreases aside from during periods of more energetic offshore wave conditions. IG wave processes have implications for sediment transport and mixing within the lagoon.